ACS APPLIED MATERIALS & INTERFACES

Research Article

www.acsami.org

Understanding the Effect of a Fluorinated Ether on the Performance of Lithium–Sulfur Batteries

Nasim Azimi,[†] Zheng Xue,[†] Ira Bloom,[†] Mikhail L. Gordin,[‡] Donghai Wang,[‡] Tad Daniel,[§] Christos Takoudis,[§] and Zhengcheng Zhang*,[†]

[†]Chemical Sciences and Engineering Division, Argonne National Laboratory, 9700 S. Cass Avenue, Argonne, Illinois 60439, United States

[‡]Department of Mechanical and Nuclear Engineering, The Pennsylvania State University, University Park, Pennsylvania 16802, United States

[§]Research Resources Center, Department of Chemical Engineering and Bioengineering, University of Illinois at Chicago, Chicago, Illinois 60607, United States

Supporting Information

ABSTRACT: A high performance Li–S battery with novel fluoroether-based electrolyte was reported. The fluorinated electrolyte prevents the polysulfide shuttling effect and improves the Coulombic efficiency and capacity retention of the Li–S battery. Reversible redox reaction of the sulfur electrode in the presence of fluoroether TTE was systematically investigated. Electrochemical tests and post-test analysis using HPLC, XPS, and SEM/EDS were performed to examine the electrode and the electrolyte after cycling. The results demonstrate that TTE as a cosolvent mitigates polysulfide dissolution and promotes conversion kinetics from polysulfides to Li_2S/Li_2S_2. Furthermore, TTE participates in a redox reaction on both electrodes, forming a solid electrolyte interphase (SEI) which further prevents parasitic reactions and thus improves the utilization of the active material.

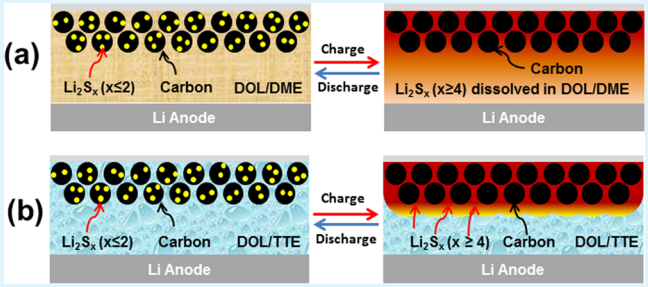

KEYWORDS: *lithium–sulfur batteries, fluorinated electrolyte, polysulfide shuttle dissolution, solid–electrolyte interphase, lithium anode passivation*

1. INTRODUCTION

Rechargeable lithium-ion batteries have been one of the best candidates for energy storage applications over the past two decades; however, at present these batteries cannot offer a suitably long driving range (i.e., >300 km) for pure electric vehicles due to their limited energy density of about 200–250 Wh kg^{-1}.[1−3] The lithium–sulfur (Li–S) battery has recently attracted attention due to its potential to meet the performance requirements for high-energy-density batteries in emerging electronics and vehicle applications.[4−9] Sulfur is a naturally abundant element, nontoxic, and one of the cheapest energy storage materials with an extremely high capacity of 1675 mAh g^{-1}.[10−12] In a Li–S cell, sulfur is electrochemically reduced to polysulfide intermediates through a multistep process, where the longer chain polysulfides tend to dissolve in the organic electrolyte.[13−17] Insoluble discharge products such as Li_2S_2 and Li_2S are generated through the reduction reactions at the final step. During the charging step, Li_2S/Li_2S_2 is converted to elemental sulfur through multiple oxidation steps.

The dissolution of the intermediate lithium polysulfides during cycling causes a severe redox shuttling effect and rapid capacity fading, which are the main obstacles for commercialization of Li–S batteries.[6,7,18] A firm understanding of the operation mechanism of the Li–S battery and the technical solution to solve these issues are in great demand in order to successfully develop Li–S batteries for commercial application.[19,20] Much research has been undertaken to overcome these problems. One approach was to introduce porous carbon materials into the cathode to trap lithium polysulfides within the cathode during cycling by the strong adsorption property of carbon.[21,22] Another approach was to form a protective layer on the lithium anode surface to mitigate the redox reaction of the dissolved polysulfides and lithium metal.[23,24] Yet another approach was the development of new solid-state electrolyte,[25,26] electrolytes consisting of ionic liquid,[27−29] tetra(ethylene glycol) dimethyl ether[30,31] as organic solvents for the electrolyte, lithium salt electrolytes,[32] and functional electrolyte/additives[33−35] to prevent the dissolution of the polysulfides into the organic electrolyte and thereby avoid the redox shuttling effect. These approaches can improve the Li–S performance to some extent but still cannot solve the above-mentioned problems.

Received: February 13, 2015
Accepted: April 13, 2015
Published: April 13, 2015

DOI: 10.1021/acsami.5b01412
ACS Appl. Mater. Interfaces 2015, 7, 9169–9177

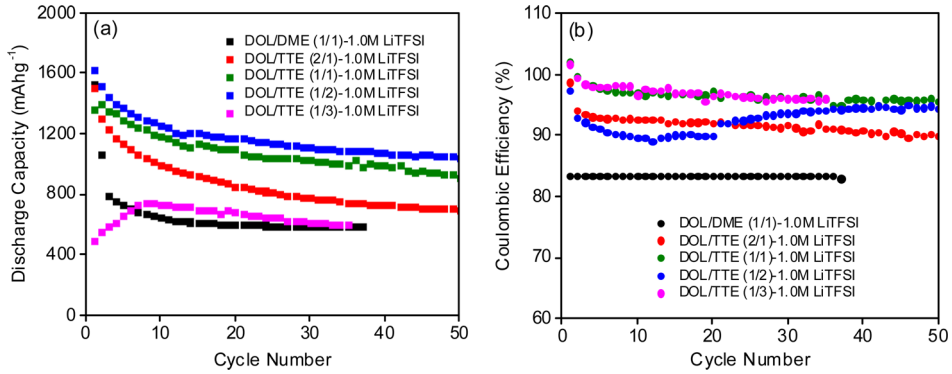

Figure 1. (a) Discharge capacity retention and (b) Coulombic efficiency profiles of Li−S cells containing baseline electrolyte 1.0 M LiTFSI DOL/DME (1/1) and fluorinated electrolyte 1.0 M LiTFSI DOL/TTE (2/1), 1.0 M LiTFSI DOL/TTE (1/1), 1.0 M LiTFSI DOL/TTE (1/2), and 1.0 M LiTFSI DOL/TTE (1/3).

In this paper, we report in detail the enhancement of the electrochemical performance of a new Li−S battery electrolyte based on organic fluorine ether as cosolvent. The new electrolyte can prevent the shuttling effect of polysulfides and significantly improve the cell performance. To understand the function mechanism behind the performance, the electrode and electrolyte were studied systematically using electrochemical methods and analytical techniques such as high-performance liquid chromatography (HPLC), X-ray photoelectron spectroscopy (XPS), and scanning electronic microscopy (SEM)/energy-dispersive X-ray spectroscopy (EDS).

2. EXPERIMENTAL SECTION

2.1. Sulfur Electrode Fabrication. A sulfur−carbon nanocomposite was prepared by impregnating sulfur into a microsized spherical nanoporous carbon.[36] Cathodes for Li−S coin cell tests were prepared by mixing 80 wt % of the carbon/sulfur composite (75% sulfur), 10 wt % carbon black (Super-P), and 10 wt % poly(vinylidene difluoride) (PVDF) dissolved in 1-methyl-2-pyrrolidinone (NMP) to form a homogeneous slurry. The slurry was then coated onto an aluminum foil current collector. The coated electrodes were dried at 60 °C under vacuum for 12 h and punched into discs with an area of 1.27 cm^2. The electrodes had 56% sulfur with loadings of 5 mg cm^{-2}.

2.2. Electrolyte Preparation. 1,1,2,2-Tetrafluoroethyl-2,2,3,3-tetrafluoropropyl ether (TTE) was purchased from Synquest Laboratories, Inc. 1,2-Dimethoxyethane (DME) and 1,3-dioxolane (DOL) were purchased from Sigma-Aldrich. All solvents were purified by vacuum distillation before use. Lithium bis-(trifluoromethanesulfonyl)imide (LiTFSI), sulfur, and Li_2S were from Sigma-Aldrich and used as received. The preparation of lithium polysulfide (Li_2S_8) in different DOL/TTE mixture solvents and electrolyte preparation were performed in an Ar-filled glovebox with controlled moisture content <5 ppm. The electrolytes tested in this study were (1) a baseline electrolyte of 1.0 M LiTFSI in DOL/DME (v:v=1:1) and (2) 1.0 M LiTFSI in DOL/TTE with various volume ratios (2:1, 1:1, 1:2, and 1:3). Complete dissolution of LiTFSI was achieved with all the solvent combinations expect for DOL/TTE (1:3), which remained slightly cloudy after prolonged stirring. The preparation of lithium polysulfide (Li_2S_4 and Li_2S_6) catholytes at different concentrations was adopted from a method of Rauh et al.[37] by mixing stoichiometric amounts of elemental sulfur and Li_2S in DOL/DME or DOL/TTE solutions.

2.3. Electrochemical Evaluation. An amount of 2032 coin cells was assembled with lithium as the anode and the above sulfur electrode as cathode. The cells were assembled in an Ar-filled glovebox and cycled with C/10 (1C = 1675 mA g^{-1}) current on a Maccor series 4000 cycler with a 1.6−2.6 V voltage range. The charging process was terminated by a cutoff voltage of 2.6 V for all the DOL/TTE electrolyte cells; for the baseline cell, the charging was terminated when the charging capacity equals 120% of the discharge capacity of the last cycle.

2.4. Electrode Surface and Morphology Characterization. The sulfur electrode was harvested from the Li−S cells after different numbers of charge−discharge cycles. The cells were disassembled inside the glovebox, and the sulfur cathode was thoroughly rinsed with electrolyte solvents and dried. The elemental characteristics, chemical state, and quantity of the element on the surface of the cathode were determined by X-ray photoelectron spectroscopy (XPS). These analyses were performed on a monochromatic Al Kα source instrument (Kratos, Axis 165, England) operated at 12 kV and 10 mA for an X-ray power of 120 W. Spectra were collected with a photoelectron takeoff angle of 90° from the sample surface plane, energy steps of 0.1 eV, and a pass energy of 20 eV for all elements. All spectra were referenced to the C 1s binding energy at 284.8 eV.

For SEM/EDS analysis, the electrode samples were loaded onto an airtight SEM sample holder. The morphology of the electrodes was examined by a high resolution JEOL JSM6610 scanning electron microscopy (SEM) operated at 5−10 kV for imaging and 10−20 keV for EDS data.

2.5. Polysulfide Dissolution Analysis. Cycled cells were disassembled inside the glovebox, and the electrolyte was collected by thoroughly rinsing the cathode and separator with dry, deoxygenated DOL. The solution was passed through a 2 μm poly(tetrafluoroethylene) filter to remove residual solids. High-performance liquid chromatography (HPLC) was used for separation of the components in a cycled electrolyte. The HPLC (Agilent 1260 Infinity) consisted of an autosampler, a degasser, a quaternary pump, and a diode array detector (190−950 nm, in steps of 1 nm). The diode array detector (DAD) was used for the qualitative and quantitative determination of the different species. Dry, deoxygenated DOL was also used as the mobile phase. In a typical experiment, the solvent reservoir was filled in an Ar-filled glovebox and capped with two layers of parafilm. It was quickly transferred to the Ar-filled glovebag, which had been purged five times with Ar and placed in the bag under a positive flow of Ar. Again, the glovebag was purged with Ar. Positive Ar pressure was maintained throughout the HPLC experiment. A Zorbax ODS column (250 × 4.6 mm), which was thermostated at 25 °C, was used to separate the electrolyte solution. The flow rate of the mobile phase was 0.5 mL min^{-1}. Between 1.0 and 50 μL of the electrolyte solution was injected by the autosampler.

3. RESULTS AND DISCUSSION

3.1. Electrochemical Performance. Fluorinated ethers were reported by Ishikawa et al.[38,39] and Nikajima et al.[40,41] for the lithium-ion battery to enhance the formation of the protection layer against further decomposition of the electrolyte at the positive electrode surface. In this paper, we investigated the effect of fluorinated ether TTE as a cosolvent on the performance of the Li−S battery.

DOI: 10.1021/acsami.5b01412
ACS Appl. Mater. Interfaces 2015, 7, 9169−9177

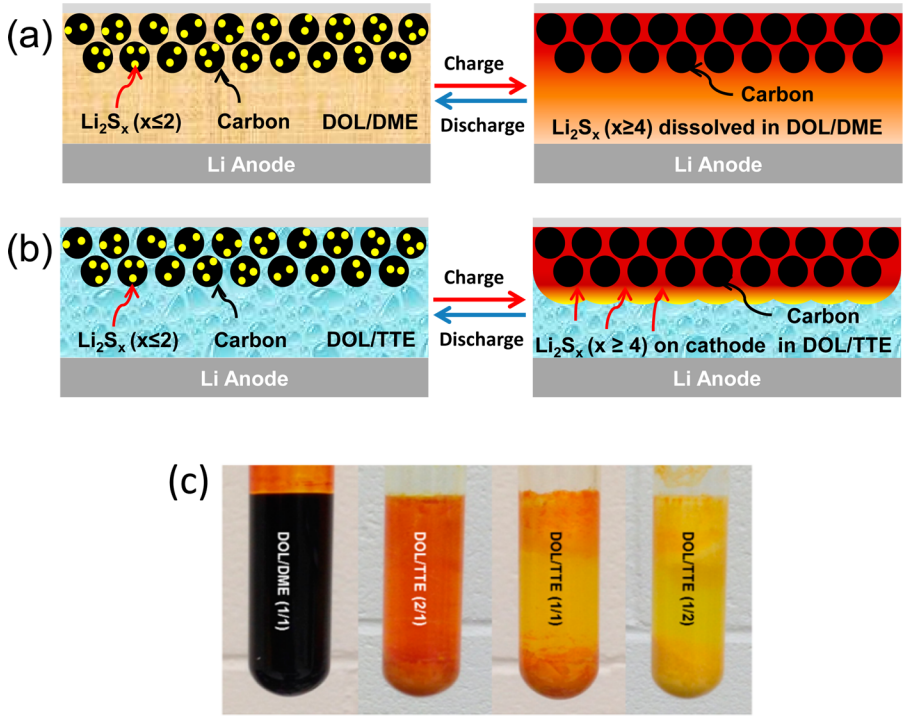

Figure 2. Schematic illustration of discharge and charge process in Li–S battery with (a) baseline electrolyte DOL/DME–1.0 M LiTFSI, (b) fluorinated electrolyte DOL/TTE–1.0 M LiTFSI, and (c) polysulfide solubility test in fluorinated electrolyte solvents: 1.0 M Li_2S_8 (based on stoichiometric amounts of Li_2S and sulfur) dissolved in baseline solvent DOL/DME (1/1) (left) and fluorinated solvents with different DOL/TTE volumetric ratios DOL/TTE (2/1) (second left), DOL/TTE (1/1) (second right), and DOL/TTE (1/2) (right).

To systematically study the fluorinated electrolyte concentration effect on battery performance, fluorinated electrolytes with different ratios of DOL to fluoroether TTE were formulated with 1.0 M LiTFSI. Figure 1a shows the capacity retention of Li–S cells in a voltage window of 1.6–2.6 V at C/10 (1C = 1675 mA g^{-1}) using electrolytes with different DOL/TTE volume ratios. The cell containing the electrolyte with a DOL/TTE ratio of 1:2 shows the best capacity retention after 50 cycles, whereas the baseline cell containing the conventional DOL/DME (1:1) electrolyte has the lowest capacity after the same number of cycles. Surprisingly, even without the use of the widely adopted $LiNO_3$ additive, the cells containing fluorinated electrolytes showed very high Coulombic efficiency, as shown in Figure 1b. Among all the TTE-containing electrolytes, the one with DOL/TTE = 1:1 showed the highest Coulombic efficiency of 97%, which contrasts with the low efficiency of 83.3% for the baseline cell. All the cells with fluorinated electrolytes can be charged to 2.6 V cutoff voltage; however, without $LiNO_3$ additive, the baseline cell was not able to reach 2.6 V due to the severe shuttling effect. The charge process had to be terminated when the charge capacity reached 120% of the previous discharge capacity. It is concluded that a higher ratio of TTE in the electrolyte leads to less dissolution of polysulfides in the electrolyte and thus suppresses their shuttling behavior. The function mechanism is proposed and schematically illustrated in Figure 2a and Figure 2b. The high solubility of polysulfides in conventional DOL/DME-based electrolyte results in diffusion of the polysulfide species into the electrolyte, and their reduction and chemical side reactions at the anode side cause a severe shuttling phenomenon and loss of active materials. However, the polysulfide intermediates have low solubility in the TTE electrolyte and tend to accumulate inside the electrode scaffold. As a result, their migration to the anode side and subsequent parasitic reactions with Li become less likely. To confirm the effect of fluorinated solvent on the cell performance, a solubility test was conducted by synthesizing 1.0 M Li_2S_x (Li_2S_x, x = 8 based on stoichiometric amounts of Li_2S and S) in DOL/DME and DOL/TTE solvents according to the method reported by Rauh et al.[37] The images for different mixtures after 48 h of agitation at 70 °C are shown in Figure 2c. It was found that Li_2S_8 completely dissolved in DOL/DME solvent to form a dark-brown and viscous solution. In contrast, less dissolution and more precipitate were observed for the mixtures with an increasing TTE ratio in the DOL/TTE solvents, as indicated by the lighter color of the mixture (the pictures of the filtered solution are shown in Figure S1, Supporting Information). The solvent mixture with the highest fluoroether concentration (DOL/TTE = 1:3) has the lowest solubility of polysulfides; however, it should be noted that the high ratio of DOL/TTE also has a significant effect on the solubility of the LiTFSI salt. The low solubility of polysulfide and LiTFSI was believed to account for the poor cell performance of DOL/TTE = 1:3 electrolyte (Figure 1a).

Figure 3 shows the first charge/discharge voltage profiles of Li–S cells with fluorinated electrolytes. Overpotential was observed in both a higher-order and lower-order plateau from charge and discharge curves for the fluorinated electrolyte cells. This is caused by the lower ionic conductivity of the fluorinated electrolytes (Figure S2, Supporting Information). Interestingly, for the TTE electrolyte cells, the contribution to the overall capacity from the higher-order polysulfide reduction (the first plateau on discharge profile at ~2.3 V) became smaller with the increasing amount of TTE. For the baseline cell, the contribution from the higher-order plateau was 570 mAh g^{-1}, which decreased to 410 mAh g^{-1} for DOL/TTE (2:1), 200 mAh g^{-1} for DOL/TTE (1:1), 260 mAh g^{-1} for DOL/TTE

DOI: 10.1021/acsami.5b01412
ACS Appl. Mater. Interfaces 2015, 7, 9169–9177

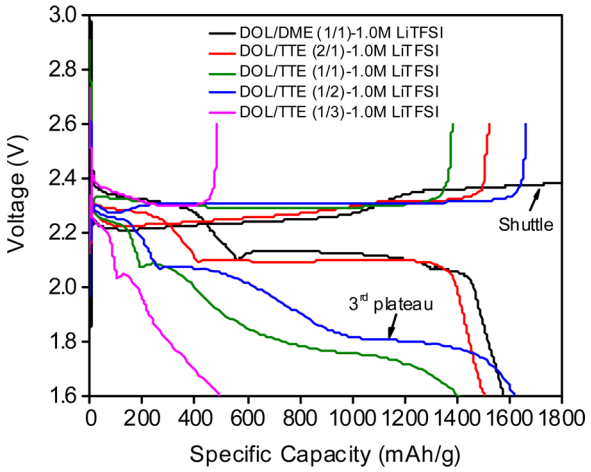

Figure 3. First charge and discharge voltage profiles for the Li−S cell containing DOL/DME (1/1)−1.0 M LiTFSI and four fluorinated electrolytes with different DOL/TTE ratios 2/1, 1/1, 1/2, and 1/3.

(1:2), and 100 mAh g^{-1} for DOL/TTE (1:3). These results imply that the reduction reaction from elemental S to higher-order polysulfides is transient and further conversion of the higher-order polysulfides to lower-order ones is more favorable in the fluorinated electrolytes than in DOL/DME-based electrolyte. Furthermore, a third plateau was observed for the electrolytes containing higher ratios of TTE (DOL/TTE, 1:1, 1:2, and 1:3), as indicated by the arrow on the discharge profile corresponding to DOL/TTE (1:2). This plateau may be related to the overpotential as well as wettability of the electrode when a high ratio of TTE is present. On the other hand, this third plateau may also be associated with the reductive decomposition of TTE on the surface of the sulfur/carbon particles during discharge, forming a passivation layer as the so-called solid−electrolyte interphase (SEI).[35] The SEI acts as a protection layer on the cathode surface and further mitigates the dissolution of the polysulfides. This finding is consistent with the SEM observation which will be discussed later.

3.2. Lithium Polysulfide Characterization. Ex situ analysis methods such as HPLC and UV−vis spectroscopy were employed to characterize the active species in the electrolyte after cycling. The standard polysulfide samples of Li_2S_4 and Li_2S_6 with different molar concentrations were first measured by HPLC. Figure 4 shows the HPLC chromatograms of standard Li_2S_6 samples with sulfur concentration of 3.0, 6.0, 12.5, and 50.0 mM. As shown in Figure 4a, three peaks were detected at retention times of 4.8−5.0, 5.8, and 6.1 min (major peak), corresponding to the elution of polysulfides with different chain lengths and sizes for the Li_2S_6 reference sample.[15,16] Since the major peak at 6.1 min is symmetrical and well-resolved, as is the baseline around this area, its position and integrated intensity at different concentrations were used to generate the calibration plot shown as the inset of Figure 4b. On the basis of this highly linear plot, one can perform quantitative analysis of the polysulfide dissolution in the cycled baseline cell and the TTE-based electrolyte cell.

The harvested baseline and fluorinated electrolyte from a Li−S cell cycled 10 times were analyzed by HPLC using conditions identical to those for the Li_2S_6 standard sample. As shown in Figure 5, polysulfide peaks were observed for baseline and

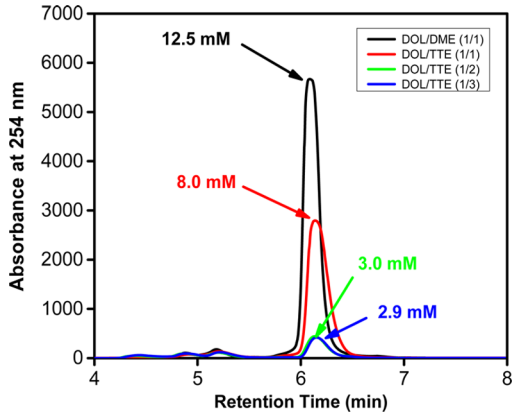

Figure 5. HPLC chromatograms of harvested electrolytes from Li−S cells after 10 cycles with DOL/DME (1/1)−1.0 M LiTFSI, DOL/TTE (1/1)−1.0 M LiTFSI, DOL/TTE (1/2)−1.0 M LiTFSI, and DOL/TTE (1/3)−1.0 M LiTFSI.

fluorinated electrolytes at 4.8, 5.2, and 6.1 min, indicating that the dissolved polysulfide species is close to Li_2S_6, not Li_2S_4 (Figure S4, Supporting Information, shows the HPLC chromatograms of Li_2S_4 standard solutions). Actually, the major peak at 6.1 min is identical to that of the Li_2S_6 standard solution. On the basis of the peak intensity and integration area at 6.1 min, the concentration of the dissolved polysulfide in the cycled cells was calculated from the calibration plot. When cycled with the baseline electrolyte, the sulfur concentration was measured to be 12.5 mM, whereas it was only 8.0, 3.0, and

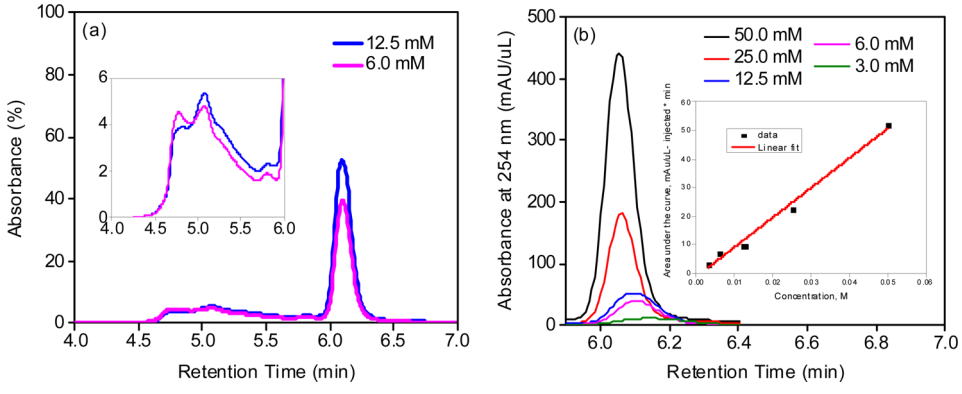

Figure 4. HPLC chromatograms of (a) Li_2S_6 reference samples and (b) Li_2S_6 reference sample major peak at 6.1 min (inset for calibration plot). The concentration is normalized to sulfur.

DOI: 10.1021/acsami.5b01412
ACS Appl. Mater. Interfaces 2015, 7, 9169−9177

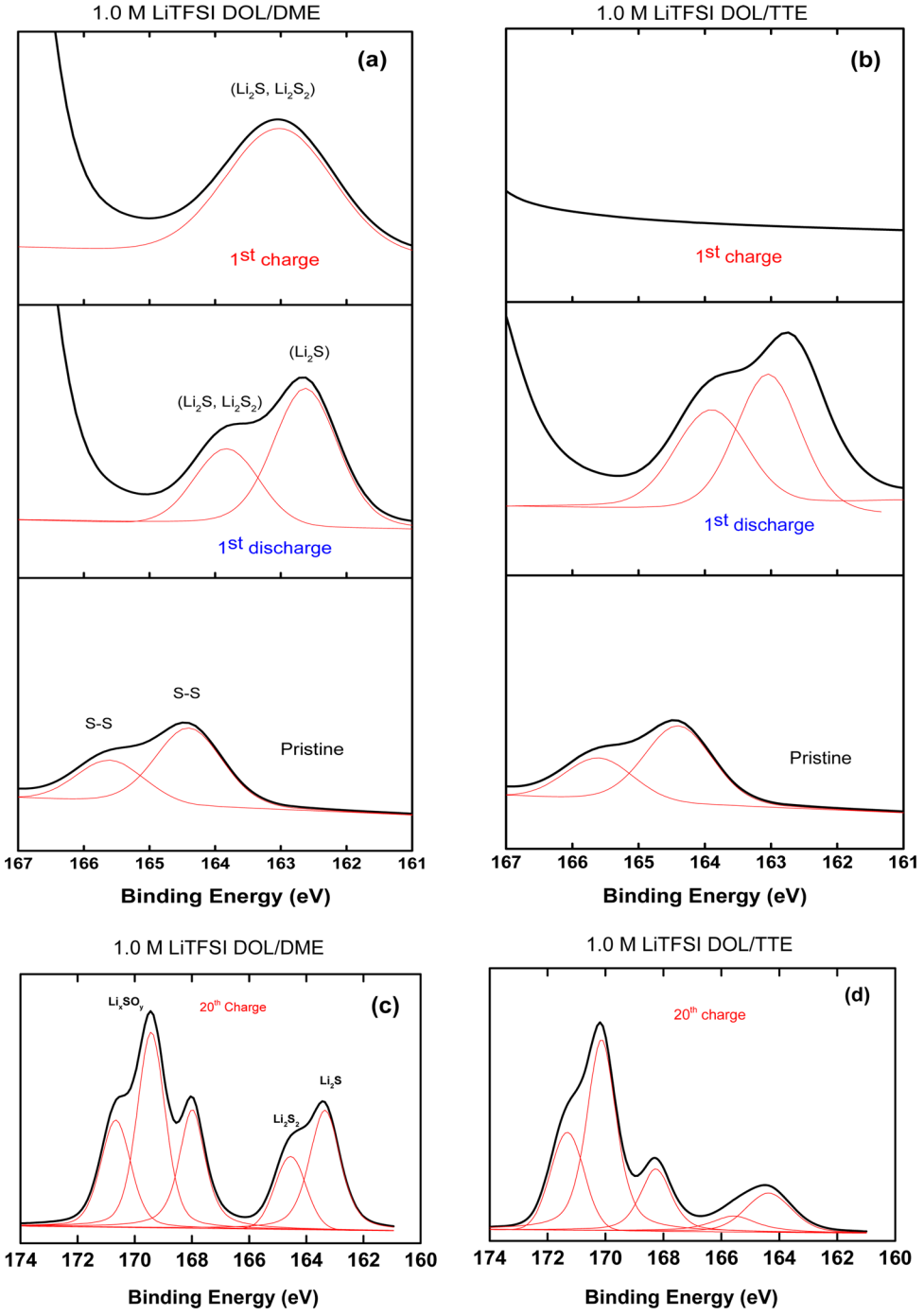

Figure 6. S_{2p} XPS spectra of sulfur electrode in pristine state, the 1st discharge state, and the 1st charge state with (a) 1.0 M LiTFSI DOL/DME (1/1) and (b) 1.0 M LiTFSI DOL/TTE (1/1); S_{2p} XPS spectra of the sulfur electrode at the 20th charge state with (c) 1.0 M LiTFSI DOL/DME (1/1) and (d) 1.0 M LiTFSI DOL/TTE (1/1).

2.9 mM for the cells with DOL/TTE/LiTFSI electrolyte with solvent ratios of 1:1, 1:2, and 1:3, respectively. Thus, when the ratio of fluorinated solvent was increased, a much lower concentration of polysulfide was generated, as well as much less diffusion of these species in the electrolyte. This finding serves as direct evidence for the improved performance the the Li−S cell in terms of Coulombic efficiency, sulfur utilization, and capacity retention with the fluorinated electrolyte.

3.3. Electrode Surface and Morphology. Previous reports by other groups have constructed a complete redox reaction mechanism of Li−S cells via impedance analysis,[42] in situ X-ray diffraction,[14,19] ex-situ SEM,[14,42,43] UV−vis absorption spectroscopy,[15] and XPS for Li anode,[44] but only a few papers reported XPS analysis on the sulfur cathode.[45,46] To further understand the effect of fluorinated solvents on the Li−S battery performance, we performed XPS analysis of the surface of cathodes retrieved from cycled cells. Figure 6a shows the S_{2p} binding energy of pristine and cycled sulfur electrodes in DOL/DME electrolyte. The S_{2p} peaks at 164.4 and 165.7 eV are characteristic of S−S bonds of elemental S_8 in the pristine cathode.[45,46] After the first discharge, the S−S peak disappeared, and two new peaks emerged in the lower energy

DOI: 10.1021/acsami.5b01412
ACS Appl. Mater. Interfaces 2015, 7, 9169−9177

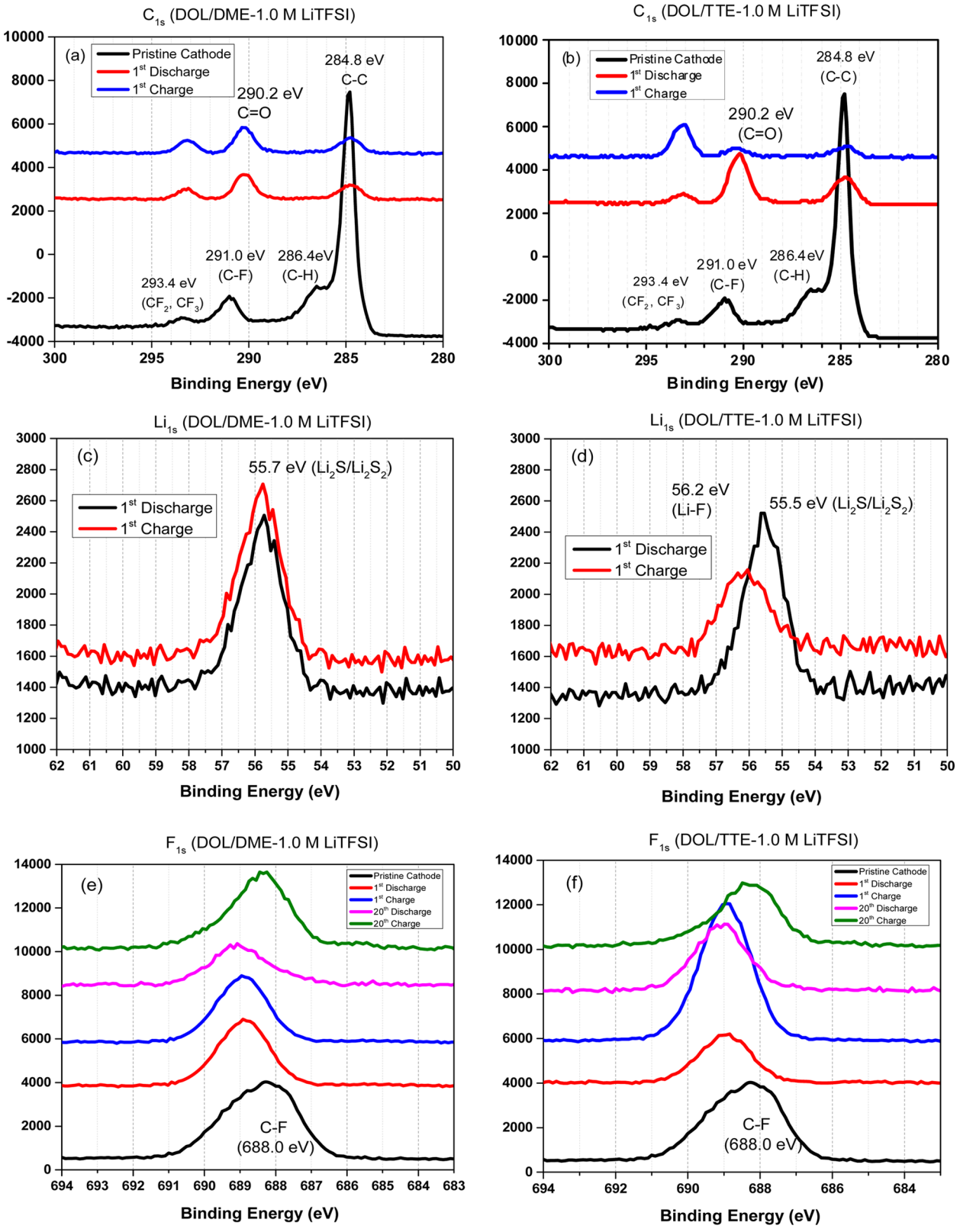

Figure 7. XPS spectra of sulfur cathodes in pristine state, the 1st discharge state, the 1st charge state, the 20th discharge state, and the 20th charge state cycled with DOL/DME (1/1)−1.0 M LiTFSI electrolyte (a) C_{1s}, (c) Li_{1s}, (e) F_{1s} and cycled with DOL/TTE (1/1)−1.0 M LiTFSI electrolyte (b) C_{1s}, (d) Li_{1s}, (f) F_{1s}.

area at 162.6 and 163.8 eV, confirming the conversion of elemental S to S^{2-} through electrochemical reduction with generation of the discharge product Li_2S or Li_2S_2,[47] and these peaks remain unchanged even in fully charged state, indicating the loss of the active material due to this irreversible reaction. However, for the electrode cycled in DOL/TTE electrolyte, the S_{2p} peaks at 162.6 and 163.8 eV in the first discharge completely vanished at the first charge, as shown in the top

DOI: 10.1021/acsami.5b01412
ACS Appl. Mater. Interfaces 2015, 7, 9169−9177

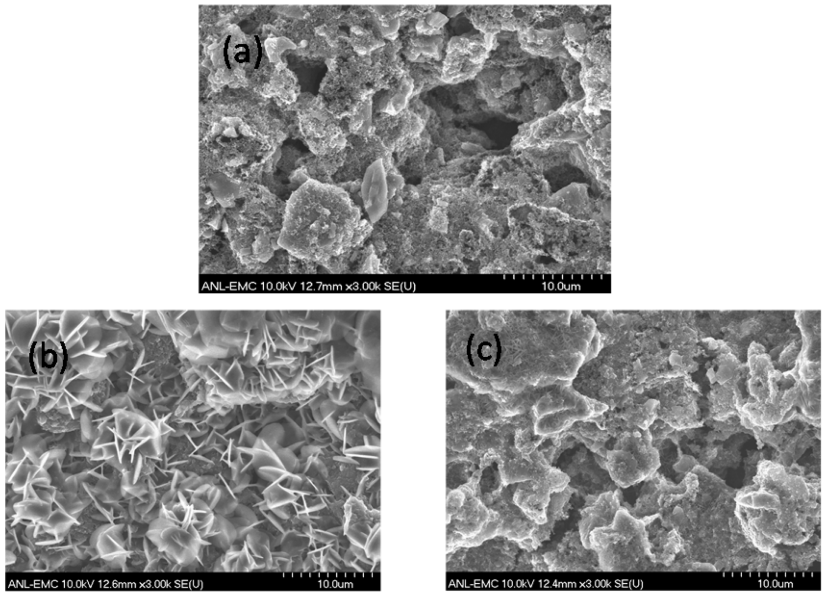

Figure 8. SEM images of (a) pristine sulfur electrode, (b) the 1st discharged sulfur electrode with 1.0 M LiTFSI DOL/DME (1/1) electrolyte, and (c) the 1st discharged sulfur electrode with 1.0 M LiTFSI DOL/TTE (1/1) electrolyte.

curve in Figure 6b. This highly reversible process explains the high specific capacity and Coulombic efficiency of the DOL/TTE-containing cell, as discussed in Sulfur Electrode Fabrication (section 2.1). The lower oxidation S_{2p} peaks exist throughout the cycling and accumulate with cycling for the DOL/DME-containing cell (Figure 6c); however, the electrochemical reversibility is maintained with the depth of cycling for the DOL/TTE-containing cell. No recognizable peaks appeared until the 20th cycle, as seen from Figure 6d, and the intensity of these S_{2p} peaks was still small when DOL/TTE was used as electrolyte. This observation is in good agreement with the improved specific capacity and capacity retention of the DOL/TTE-containing cell. As evident in Figure 7c and 7d, additional sulfur peaks appeared for cells with the baseline and fluorinated electrolytes at the higher binding energy range (168, 169, and 171 eV). They arise from the formation of Li_xSO_y species due to the reaction of the LiTFSI with the active material.[45,46] The intensity of these peaks increases with cycling, leading to the deterioration of the cell performance.

The C_{1s}, Li_{1s}, and F_{1s} XPS spectra of sulfur cathodes at different charge and discharging cycles are shown in Figure 7. In the pristine cathode, the C_{1s} peak at 248.8 eV was attributed to the C−C, and peaks at 286.4 and 291.0 eV (Figure 7a and 7b) were assigned to C−H and C−F bonds from the PVDF binder in the electrode.[48] At the first discharge, the C_{1s} peaks were covered by new species (C═O at 290.2 eV and CF_2 at 293.4 eV) due to the SEI formation and the deposition of the discharge products on the electrode surface. Interestingly, for the DOL/TTE-containing cell, the binding energy of the C−F peak (CF_2)[49] has high intensity, and this peak does not disappear even at the fully charged state (Figure 7b). In the Li_{1s} spectra, the peak at 55.5 eV was assigned to the Li−S bonds from Li_2S/Li_2S_2 at the discharge state for the DOL/DME-containing cell (Figure 7c) and DOL/TTE-containing cell (Figure 7d). However, in the charge state, this peak disappeared, and a new peak emerged at a shifted position at 56.2 eV, corresponding to the formation of the Li−F bond for the DOL/TTE-containing cell (Figure 7d), whereas the peak remained unchanged in terms of position and intensity for the DOL/DME-containing cell (Figure 7c). The LiF-rich SEI formed on the sulfur surface further improves the Coulombic efficiency and capacity retention.

Figure 7e and 7f shows the F_{1s} XPS profiles. Decomposition products comprising the C−F bond dominate the spectra for electrodes cycled with both electrolyte types. For the pristine sulfur electrode, the peak centered at 688 eV was attributed to the PVDF binder, and the peak shifted when LiTFSI was involved in the electrochemical reaction on the electrode surface. However, a larger contribution from C−F was observed for the electrode with DOL/TTE electrolyte (Figure 7f) due to the participation of the electrochemical reduction of the TTE solvent on the sulfur electrode.[50]

The morphology of the cycled sulfur electrode is also investigated by SEM. Figure 8a is a typical SEM image of the pristine sulfur/carbon electrode. After the first discharge in the DOL/DME electrolyte, the surface of cathode was deposited with large quantities of crystal-like discharge products (Figure 8b) of the insoluble lithium sulfides (Li_2S and/or Li_2S_2). Further analysis of the deposit by XRD and energy-dispersive X-ray spectroscopy (EDS) revealed a surface morphology with Li_2S/Li_2S_2 agglomeration. When the DOL/TTE electrolyte was used, the discharged electrode showed morphology similar to the pristine cathode filled with fine discharged product particles/flakes hidden in the porous structure of the sulfur−carbon composite, as illustrated in Figure 8c. Additionally, much less lithium polysulfide deposition was detected from the EDS spectrum. SEM results indicate that the SEI layer formation through reductive decomposition of TTE on the surface of the cathode suppressed the polysulfide dissolution and agglomeration of the discharged species, an observation that is supported by the improved specific capacity and superior Coulombic efficiency for the fluorinated electrolyte cells vs baseline cell (Figure 1 and Figure 3).

The improved performance of the fluorinated electrolyte Li−S cell is also attributed to the protection of the lithium metal anode. Aurbach et al.[44] reported that the shuttle effect can be suppressed by the addition of $LiNO_3$ additive to the DOL/DME electrolytes. $LiNO_3$ participates in the formation of a

DOI: 10.1021/acsami.5b01412
ACS Appl. Mater. Interfaces 2015, 7, 9169−9177

stable passivation film on the surface of the Li anode, which protects the dissolved polysulfides from reacting with the Li anode. However, the capacity still fades with cycling, indicating that the $LiNO_3$ could not eliminate the active material loss. TTE is thermodynamically unstable in contact with lithium metal and tends to chemically react with it. As a perfluorinated ether, TTE chemically and electrochemically reacts with lithium metal, forming a conjugated C═C bond and LiF.[51] Our SEM analysis of the lithium metal immersed in TTE solvent for 12 h revealed the formation of the LiF-rich composite layer on the Li anode surface (Figure S5, Supporting Information). This layer could serve as a physical barrier, thereby further inhibiting the chemical and electrochemical reaction of polysulfides with the Li anode.[52]

CONCLUSIONS

A deeper understanding of a high performance Li−S battery with DOL/TTE fluorinated electrolyte was gained by using electrochemical methods and various analytical techniques such as HPLC, XPS, and SEM. The lithium polysulfide species generated in a Li−S cell with this electrolyte were quantitatively analyzed. The results suggested that the improved performance of a Li−S cell with TTE as cosolvent is due to multiple reasons: (1) less solubility of higher-order polysulfides as confirmed with a solubility test and an HPLC experiment mitigates the shuttle effect of the polysulfide and promotes the reversible electrochemistry of insoluble Li_2S/Li_2S_2; (2) the SEI formation on the sulfur cathode by reductive decomposition of the fluoroether further prevents the dissolution of the polysulfide and improves sulfur utilization; (3) the electrochemical/chemical reaction of fluoroether with the lithium anode forms a protective layer, acting as a physical barrier to eliminate the parasitic reactions of dissolved polysulfides with lithium.

ASSOCIATED CONTENT

Supporting Information

Detailed experimental procedures as well as some further comments on the effect of electrolyte/sulfur ratio in this system. The Supporting Information is available free of charge on the ACS Publications website at DOI: 10.1021/acsami.5b01412.

AUTHOR INFORMATION

Corresponding Author

*Phone: (630)-252-7868. E-mail: zzhang@anl.gov.

Author Contributions

The manuscript was written through contributions of all authors. All authors have given approval to the final version of the manuscript.

Funding

This research is supported by the Vehicle Technologies Office, U.S. Department of Energy. Argonne, a U.S. Department of Energy laboratory, is operated by UChicago Argonne, LLC under contract DE-AC02-06CH11357.

Notes

The authors declare no competing financial interest.

ACKNOWLEDGMENTS

SEM/EDS analysis was performed at Electron Microscopy Center at Argonne National Laboratory, and XPS analysis was conducted at Research Resources Center at University of Illinois—Chicago.

REFERENCES

(1) Scrosati, B.; Hassoun, J.; Sun, Y.-K. Lithium-Ion Batteries. A Look into the Future. *Energy Environ. Sci.* **2011**, *4*, 3287−3295.
(2) Ji, X.; Nazar, L. F. Advances in Li−S Batteries. *J. Mater. Chem.* **2010**, *20*, 9821−9826.
(3) Thackeray, M. M.; Wolverton, C.; Isaacs, E. D. Electrical Energy Storage for Transportation−Approaching the Limits of, and Going Beyond, Lithium-ion batteries. *Energy Environ. Sci.* **2012**, *5*, 7854−7863.
(4) Scrosati, B.; Garche, J. Lithium Batteries: Status, Prospects and Future. *J. Power Sources* **2010**, *195*, 2419−2430.
(5) Wang, H.; Yang, Y.; Liang, Y.; Robinson, J. T.; Li, Y.; Jackson, A.; Cui, Y.; Dai, H. Graphene-Wrapped Sulfur Particles as a Rechargeable Lithium−Sulfur Battery Cathode Material with High Capacity and Cycling Stability. *Nano Lett.* **2011**, *11*, 2644−2647.
(6) Su, Y. S.; Fu, Y.; Cochell, T.; Manthiram, A. A Strategic Approach to Recharging Lithium-Sulphur Batteries for Long Cycle Life. *Nat. Commun.* **2013**, *4*, 2985.
(7) Chen, L.; Shaw, L. L. Recent Advances in Lithium−Sulfur Batteries. *J. Power Sources* **2014**, *267*, 770−783.
(8) Evers, S.; Nazar, L. F. New Approaches for High Energy Density Lithium−Sulfur Battery Cathodes. *Acc. Chem. Res.* **2012**, *46*, 1135−1143.
(9) Wang, L.; Byon, H. R. N-Methyl-N-propylpiperidinium Bis(trifluoromethanesulfonyl)imide-Based Organic Electrolyte for High Performance. Lithium−Sulfur Batteries. *J. Power Sources* **2013**, *236*, 207−214.
(10) Marmorstein, D.; Yu, T. H.; Striebel, K. A.; McLarnon, F. R.; Hou, J.; Cairns, E. J. Electrochemical Performance of Lithium/Sulfur Cells with Three Different Polymer Electrolytes. *J. Power Sources* **2000**, *89*, 219−226.
(11) Bruce, P. G.; Hardwick, L. J.; Abraham, K. M. Lithium-Air and Lithium-Sulfur Batteries. *MRS Bull.* **2011**, *36*, 506−512.
(12) Hofmann, A. F.; Fronczek, D. N.; Bessler, W. G. Mechanistic Modeling of Polysulfide Shuttle and Capacity Loss in Lithium−Sulfur Batteries. *J. Power Sources* **2014**, *259*, 300−310.
(13) Zhang, S. S. Liquid Electrolyte Lithium/Sulfur Battery: Fundamental Chemistry, Problems, and Solutions. *J. Power Sources* **2013**, *231*, 153−162.
(14) Cañas, N. A.; Wolf, S.; Wagner, N.; Friedrich, K. A. In-Situ X-Ray Diffraction Studies of Lithium−Sulfur Batteries. *J. Power Sources* **2013**, *226*, 313−319.
(15) Barchasz, C.; Molton, F.; Duboc, C.; Leprêtre, J.-C.; Patoux, S.; Alloin, F. Lithium/Sulfur Cell Discharge Mechanism: An Original Approach for Intermediate Species Identification. *Anal. Chem.* **2012**, *84*, 3973−3980.
(16) Kawase, A.; Shirai, S.; Yamoto, Y.; Arakawa, R.; Takata, T. Electrochemical Reactions of Lithium−Sulfur Batteries: An Analytical Study Using the Organic Conversion Technique. *Phys. Chem. Chem. Phys.* **2014**, *16*, 9344−9350.
(17) Zhang, S. S. New Insight into Liquid Electrolyte of Rechargeable Lithium/Sulfur Battery. *Electrochim. Acta* **2013**, *97*, 226−230.
(18) Zhang, S. S.; Read, J. A. A New Direction for the Performance Improvement of Rechargeable Lithium/Sulfur Batteries. *J. Power Sources* **2012**, *200*, 77−82.
(19) Nelson, J.; Misra, S.; Yang, Y.; Jackson, A.; Liu, Y.; Wang, H.; Dai, H.; Andrews, J. C.; Cui, Y.; Toney, M. F. In Operando X-ray Diffraction and Transmission X-ray Microscopy of Lithium Sulfur Batteries. *J. Am. Chem. Soc.* **2012**, *134*, 6337−6343.
(20) Yeon, J.-T.; Jang, J.-Y.; Han, J.-G.; Cho, J.; Lee, K. T.; Choi, N.-S. Raman Spectroscopic and X-ray Diffraction Studies of Sulfur Composite Electrodes during Discharge and Charge. *J. Electrochem. Soc.* **2012**, *159*, A1308−A1314.
(21) Jeong, S.; Bresse, D.; Buchholz, D.; Winter, M.; Passerini, S. Carbon Coated Lithium Sulfide Particles for Lithium Battery Cathodes. *J. Power Sources* **2013**, *235*, 220−225.
(22) Zu, C.; Su, Y.-S.; Fu, Y.; Manthiram, A. Improved Lithium−Sulfur Cells with a Treated Carbon Paper Interlayer. *Phys. Chem. Chem. Phys.* **2013**, *15*, 2291−2297.

DOI: 10.1021/acsami.5b01412
ACS Appl. Mater. Interfaces 2015, 7, 9169−9177

(23) Chung, K.-I.; Kim, W.-S.; Choi, Y.-K. Lithium Phosphorous Oxynitride as a Passive Layer for Anodes in Lithium Secondary Batteries. *J. Electroanal. Chem.* **2004**, *566*, 263−267.
(24) Lee, Y. M.; Choi, N.-S.; Park, J. H.; Park, J.-K. Electrochemical Performance of Lithium/Sulfur Batteries with Protected Li Anodes. *J. Power Sources* **2003**, *119*−*121*, 964−972.
(25) Nagao, M.; Hayashi, A.; Tatsumisago, M. Electrochemical Performance of All-Solid-State Li/S Batteries with Sulfur-Based Composite Electrodes Prepared by Mechanical Milling at High Temperature. *Energy Technol.* **2013**, *1*, 186−192.
(26) Hassoun, J.; Scrosati, B. Moving to a Solid-State Configuration: A Valid Approach to Making Lithium-Sulfur Batteries Viable for Practical Applications. *Adv. Mater.* **2010**, *22*, 5198−5201.
(27) Yuan, L. X.; Feng, J. K.; Ai, X. P.; Cao, Y. L.; Chen, S. L.; Yang, H. X. Improved Dischargeability and Reversibility of Sulfur Cathode in a Novel Ionic Liquid Electrolyte. *Electrochem. Commun.* **2006**, *8*, 610−614.
(28) Shin, J. H.; Cairns, E. J. N-Methyl-(n-butyl)pyrrolidinium Bis(trifluoromethanesulfonyl)imide-LiTFSI−Poly(ethylene glycol) Dimethyl Ether Mixture as a Li/S Cell Electrolyte. *J. Power Sources* **2008**, *177*, 537−545.
(29) Dokko, K.; Tachikawa, N.; Yamauchi, K.; Tsuchiya, M.; Yamazaki, A.; Takashima, E.; Park, J.-W.; Ueno, K.; Seki, S.; Serizawa, N.; Watanabe, M. Solvate Ionic Liquid Electrolyte for Li−S Batteries. *J. Electrochem. Soc.* **2013**, *160*, A1304−A1310.
(30) Ryu, H.-S.; Ahn, H.-J.; Kim, K.-W.; Ahn, J.-H.; Cho, K. K.; Nam, T.-H.; Kim, J.-U.; Cho, G.-B. Discharge Behavior of Lithium/Sulfur Cell with TEGDME Based Electrolyte at Low Temperature. *J. Power Sources* **2006**, *163*, 201−206.
(31) Chang, D.-R.; Lee, S.-H.; Kim, S.-W.; Kim, H.-T. Binary Electrolyte Based on Tetra(ethylene glycol) Dimethyl Ether and 1,3-Dioxolane for Lithium−Sulfur Battery. *J. Power Sources* **2002**, *112*, 452−460.
(32) Aihara, Y.; Bando, T.; Nakagawa, H.; Yoshida, H.; Hayamizu, K.; Akiba, E.; Price, W. S. Ion Transport Properties of Six Lithium Salts Dissolved in γ-Butyrolactone Studied by Self-Diffusion and Ionic Conductivity Measurements. *J. Electrochem. Soc.* **2004**, *151*, A119−A122.
(33) Lin, Z.; Liu, Z.; Fu, W.; Dudney, N. J.; Liang, C. Phosphorous Pentasulfide as a Novel Additive for High-Performance Lithium-Sulfur Batteries. *Adv. Funct. Mater.* **2013**, *23*, 1064−1069.
(34) Cuisinier, M.; Cabelguen, P.-E.; Adams, B. D.; Garsuch, A.; Balasubramanian, M.; Nazar, L. F. Unique Behaviour of Nonsolvents for Polysulphides in Lithium−Sulphur Batteries. *Energy Environ. Sci.* **2014**, *7*, 2697−2705.
(35) Azimi, N.; Weng, W.; Takoudis, C.; Zhang, Z. Improved Performance of Lithium−Sulfur Battery with Fluorinated Electrolyte. *Electrochem. Commun.* **2013**, *37*, 96−99.
(36) Sohn, H.; Gordin, M. L.; Xu, T.; Chen, S.; Lv, D.; Song, J.; Manivannan, A.; Wang, D. Porous Spherical Carbon/Sulfur Nanocomposites by Aerosol-Assisted Synthesis: The Effect of Pore Structure and Morphology on Their Electrochemical Performance as Lithium/Sulfur Battery Cathodes. *ACS Appl. Mater. Interfaces* **2014**, *6*, 7596−7606.
(37) Rauh, R. D.; Shuker, F. S.; Marston, J. M.; Brummer, S. B. Formation of Lithium Polysulfides in Aprotic Media. *J. Inorg. Nucl. Chem.* **1977**, *39*, 1761−1766.
(38) Ishikawa, M.; Yamagata, M.; Sugimoto, T.; Atsumi, Y.; Kitagawa, T.; Azuma, K. Li-Ion Battery Performance with FSI-Based Ionic Liquid Electrolyte and Fluorinated Solvent-Based Electrolyte. *ECS Trans.* **2011**, *33*, 29−36.
(39) Kitagawa, T.; Azuma, K.; Koh, M.; Yamauchi, A.; Kagawa, M.; Sakata, H.; Miyawaki, H.; Nakazono, A.; Arima, H.; Yamagata, M.; Ishikawa, M. Application of Fluorine-Containing Solvents to $LiCoO_2$ Cathode in High Voltage Operation. *Electrochemistry* **2010**, *78*, 345−348.
(40) Ohmi, N.; Nakajima, T.; Ohzawa, Y.; Koh, M.; Yamauchi, A.; Kagawa, M.; Aoyama, H. Effect of Organo-Fluorine Compounds on the Thermal Stability and Electrochemical Properties of Electrolyte Solutions for Lithium Ion Batteries. *J. Power Sources* **2013**, *221*, 6−13.
(41) Achiha, T.; Nakajima, T.; Ohzawa, Y.; Koh, M.; Yamauchi, A.; Kagawa, M.; Aoyama, H. Thermal Stability and Electrochemical Properties of Fluorine Compounds as Nonflammable Solvents for Lithium-Ion Batteries. *J. Electrochem. Soc.* **2010**, *157*, A707−A712.
(42) Yuan, L.; Qiu, X.; Chen, L.; Zhu, W. New Insight into the Discharge Process of Sulfur Cathode by Electrochemical Impedance Spectroscopy. *J. Power Sources* **2009**, *189*, 127−132.
(43) Cheon, S.-E.; Ko, K.-S.; Cho, J.-H.; Kim, S.-W.; Chin, E.-Y.; Kim, H.-T. Rechargeable Lithium Sulfur Battery I. Structural Change of Sulfur Cathode During Discharge and Charge. *J. Electrochem. Soc.* **2003**, *150*, A796−A799.
(44) Aurbach, D.; Pollak, E.; Elazari, R.; Salitra, G.; Scordilis, C.; Affinito, J. On the Surface Chemical Aspects of Very High Energy Density, Rechargeable Li−Sulfur Batteries. *J. Electrochem. Soc.* **2009**, *156*, A694−A702.
(45) Fu, Y.; Su, Y.-S.; Manthiram, A. Highly Reversible Lithium/Dissolved Polysulfide Batteries with Carbon Nanotube Electrodes. *Angew. Chem., Int. Ed.* **2013**, *52*, 6930−6935.
(46) Diao, Y.; Xie, K.; Xiong, S.; Hong, X. Insights into Li-S Battery Cathode Capacity Fading Mechanisms: Irreversible Oxidation of Active Mass during Cycling. *J. Electrochem. Soc.* **2012**, *159*, A1816−A1821.
(47) Kim, H. S.; Arthur, T. S.; Allred, G. D.; Zajicek, J.; Newman, J. G.; Rodnyansky, A. E.; Oliver, A. G.; Boggess, W. C.; Muldoon, J. Structure and Compatibility of a Magnesium Electrolyte with a Sulphur Cathode. *Nat. Commun.* **2011**, *2*, 427.
(48) Mikhaylik, Y.; Kovalev, I.; Schock, R.; Kumaresan, K.; Xu, J.; Affinito, J. High Energy Rechargeable Li-S Cells for EV Application: Status, Remaining Problems and Solutions. *ECS Trans.* **2010**, *25*, 23−24.
(49) Palchan, I.; Crespin, M.; Estrade-Szwarckopf, H.; Rousseau, B. Graphite Fluorides: An XPS Study of a New Type of C-F Bonding. *Chem. Phys. Lett.* **1989**, *157*, 321.
(50) Dillon, E. P.; Crouse, C. A.; Barron, A. R. Synthesis, Characterization, and Carbon Dioxide Adsorption of Covalently Attached Polyethyleneimine-Functionalized Single-Wall Carbon Nanotubes. *ACS Nano* **2008**, *2*, 156−164.
(51) Kavan, L. Electrochemical Carbon. *Chem. Rev.* **1997**, *97*, 3061−3082.
(52) Gordin, M. L.; Dai, F.; Chen, S.; Xu, T.; Song, J.; Tang, D.; Azimi, N.; Zhang, Z.; Wang, D. Bis(2,2,2-trifluoroethyl) Ether as an Electrolyte Cosolvent for Mitigating Self-Discharge in Lithium−Sulfur Batteries. *ACS Appl. Mater. Interfaces* **2014**, *6*, 8006−8010.

DOI: 10.1021/acsami.5b01412
ACS Appl. Mater. Interfaces 2015, 7, 9169−9177